HIGH SCHOOL EDITION
Journal of Student Research
Volume 13 Issue 4 (2024)

A Novel 3D-Printed Implant for Neuroglial Regeneration: Advancing Central Nervous System Recovery

Iris Fan

American Heritage School, USA

ABSTRACT

Neurological disorders, including traumatic brain injuries (TBIs), spinal cord injuries (SCIs), peripheral nerve injuries (PNIs), and neurodegenerative disorders (NDs), affect 1 in 6 individuals globally. The central nervous system (CNS) has a limited regenerative capacity following injury or disease leaving long-lasting cognitive dysfunction. The field's current gold standard, nerve grafts, poses risks of infection, functional limitations, and substantial costs. Neuroglia, specifically astrocytes with distinct A1 and A2 categories play a crucial role in homeostasis and neurogenesis in the CNS. A1 reactive astrocytes induce neuron death while A2 reactive astrocytes promote neuron growth. This investigation aimed to enhance CNS recovery by developing a 3D-printed hydrogel-integrated scaffold. A novel scaffold was printed with polyethylene terephthalate glycol (PETG) chemically crosslinked with a gelatin/chitosan/silk fibroin hydrogel incorporated with nerve growth factor (NGF) and chondroitinase ABC (ChABC) to stimulate nerve growth and mitigate tissue scarring. Biomaterial and biological characterization was done against the positive control, a murine nerve graft. An SEM analysis indicated a 75μm pore size and a porosity appropriate for astrocyte growth. A rheological frequency sweep found a complex modulus up to 162 Pascals. The implant absorbed water up to 92% of its dry mass and exhibited slow degradability. Cell growth increased 167% within a 3-day period with 94% cell viability. The implant also displayed a significantly lower amount of neuroinflammatory markers and axon growth of 45μm. Overall, this novel integrated implant holds promise for CNS regeneration and neural engineering applications, offering a biocompatible, functional, cost-effective alternative to current standards.

Introduction

The human brain is highly vulnerable to injury, which poses a significant risk of cognitive dysfunction and lowered quality of life. Injuries to the central nervous system (CNS) encompass traumatic brain injuries (TBIs), spinal cord injuries (SCIs), stroke, and neurodegenerative diseases such as Parkinson's Disease and Alzheimer's Disease. TBIs are defined as brain dysfunction through an outside force, usually through blunt force. TBIs are some of the most frequent causes of morbidity and mortality in both developed and developing countries. The World Health Organization (WHO) has estimated that 57 million people have been hospitalized from TBIs and 52,000 die annually from TBI in the United States (Smith, 2018). SCIs consist of any damage inflicted upon the nerves of the spinal cord. Between 250,000 to 500,000 people suffer from SCI every year. Individuals who suffer from SCIs are two to five times more likely to die prematurely compared to individuals without SCIs (World Health Organization, 2013). Stroke, or cerebrovascular accident (CVA), results from interrupted blood supply to the brain and afflicts approximately 15 million individuals annually, in the world (World Health Organization, 2023). Neurodegenerative diseases are those in which cells of the CNS degenerate or die and include Parkinson's Disease, Alzheimer's Disease, Huntington's Disease, Multiple Sclerosis, and Amyotrophic Lateral Sclerosis (ALS). Around 50 million people suffer from epilepsy and 24 million from Alzheimer's every

year globally (World Health Organization, 2007). All of these CNS injuries have an associated long recovery time and high financial burden. For instance, TBIs can result in a cost of up to $56 billion a year and can trigger neurodegenerative diseases (Tian et al., 2014). The expenses for SCIs can be greater than $1 million for the first year of treatment. Stroke-related costs reached almost $56.5 billion in the United States between 2018 and 2019 (Centers for Disease Control, 2023). In addition, the economic cost of neurological disorders was 139 billion euros in Europe in 2004 (World Health Organization, 2007). Overall, CNS injuries generate large societal and economic burdens across the globe.

The vertebrate nervous system consists of two main parts: the CNS and the peripheral nervous system (PNS). The CNS comprises the brain and the spinal cord while the PNS is a collection of nerves that are found throughout the entire vertebrate body. Neurons and neuroglia are two main cell categories of the nervous system. Neurons are composed of soma, axons, and dendrites. Dendrites send electrical signals received from neural cells to the soma and axons conduct impulses away from the soma. Neuroglia are support cells, are much more plentiful than neurons, and have the ability to divide. Astrocytes and oligodendrocytes are found in the CNS while Schwann cells are located in the PNS. Every injury towards the nervous system shares a common feature of a loss of neurons and supporting cells as well as demyelination and injury of the axon (Tian et al., 2014). The process of remyelination is a regenerative process within the CNS but lacks effective therapy (Quan et al., 2022). Recent studies have investigated the role of glial cells underlying remyelination and axon regeneration. Astrocytes are ubiquitous within the CNS and play a role in regulating the blood-brain barrier and formation of synapses(Li et al., 2018). In specific, the role of reactive astrocytes has been heavily studied for a potential role for differentiation into NSCs and neuronal regeneration (Gallo and Deneen, 2014). Reactive astrocytes are most often classified into two categories: A1 and A2 reactive astrocytes. A1 reactive astrocytes are proinflammatory and induce neuron death while A2 astrocytes are anti-inflammatory and promote growth of neurons and synapse repair (Liddelow and Barres, 2017). A2 reactive astrocytes support growth of regenerating axons by guiding their elongation and bridging spinal cord slumps (Ohtake et al., 2016). Due to these properties, A2 reactive astrocytes have potential to be utilized for neuronal regeneration.

Neural tissue and repair have garnered attention in the past few years since it is crucial to the patient's quality of life. Autologous nerve grafts, which utilizes sacrificial nerves from another part of the body, are the current gold standard to treat neural defects. However, the limitations of autologous nerve grafts consist of a short age of the nerves, a mismatch between the donor and the site, formation of neuroma, and lack of functional recovery (Subramanian et al., 2009). Another option of allogeneic grafts, isolated from cadavers, has also been utilized but these suffer from host-graft immune rejection. High costs upwards of thousands of dollars also impacts a large economic burden onto patients (Ansaripour et al., 2023). Recent advances have explored the use of polymeric biomaterial scaffolds for peripheral and central nerve regeneration. These scaffolds display a wide range of available polymers that display different properties. Hydrogels are water-swollen and cross-linked polymeric networks produced by the reaction of one or more monomers. These have properties of flexibility and a similarity to natural tissues due to their large water content and exhibition of a 3D structure to the extracellular matrix (ECM). Hydrogels are considered to be an ideal carrier system for various biomedical applications including nerve repair. Hydrogels exhibit many advantages in the application of nervous system repair, as they possess good biodegradability, high moisture content, adjustable mechanical strength, abundant pore space, and have been widely studied (Ma et al., 2022). Hydrogels can be divided into two categories: natural-based biomaterials and synthetic biomaterials. Despite the numerous benefits of hydrogels, they also have some downsides. For instance, natural-based polymers can have poor mechanical properties, and it is hard to purify them for large-scale production. Synthetic polymers lack biocompatibility and a bioactive sequence. Due to these drawbacks, utilizing synthetic biomaterials that are modified with natural polymers improves the efficacy of the hydrogel (Ma et al., 2022). Gelatin and silk fibroin are two protein, natural hydrogels that have significant advantages for neural repair and regeneration due to remarkable biocompatibility, ECM mimicry, and biodegradability (Krishani et al., 2023). Chitosan is a polysaccharide, natural hydrogel and has additional

neuroregenerative properties (Ma et al., 2022). Polyethylene glycol (PEG) is a great synthetic polymer for neural repair that makes up for the lack of mechanical properties of natural hydrogels. All of these hydrogels contain properties of neuron and axon regeneration, neural repair, and promote survival. There are a series of cross linking methods available for preparation of hydrogel scaffolds. Genipin has been shown to be a very effective cross linking chemical for elasticity and porous properties (Wang et al., 2020).

A comprehensive selection of novel biomaterials to create an integrated implant capable of mimicking tissue and promoting axon growth was constructed. Specifically, a synthetic scaffold made of polyethylene terephthalate glycol (PETG) chemically crosslinked with a gelatin/chitosan/silk fibroin hydrogel loaded with particles of NGF and ChABC was designed. Using the regenerative potential of A2 reactive astrocytes, the study aims to achieve recovery and repair in the central nervous system (CNS) through the development of a novel 3D-printed implant designed to support neuroglial regeneration. It was hypothesized that If a synthetic 3D printed polymer is integrated with natural polymers, then it will yield properties of a beneficial regenerative nerve scaffold, and that If reactive astrocytes are used to promote regeneration, then it will stimulate proliferation of neurons and support axon growth. The engineering goals were to ensure that the implant would be porous, three-dimensional, biodegradable, biocompatible, noninflammatory, non-toxic, and cost-effective.

Materials + Methods

Cell Culture and Differentiation

SIM-A9 Mouse microglial cells (ATCC) and C8-D1A Mouse astrocyte cells (ATCC) were incubated in T75 cell culture flasks in a 37°C incubator at 5% CO_2. DMEM/F12 supplemented with 10% Fetal Bovine Serum (FBS), 1% Penicillin/Streptomycin (P/S) were used for the C8D1A and differentiated cells. DMEM/F12 supplemented with 10% FBS, 5% Horse Serum (HS), 1% P/S were used for the SIM-A9 cells. Cells were checked daily using a cell imager. Cell medium was changed every 2-3 days (when medium looks slightly orange). Medium was changed by removing and discarding the cell medium inside the flask and adding 10mL of fresh, pre-warmed medium into the flask. Cells were passaged when 70-80% confluency was reached. A solution of 1L-4 cytokine was added to ensure that the microglial cell medium has a concentration of 40ng/mL. Gently rock the flask back and forth to mix well. The previous medium in the microglial cell flasks were removed and discarded. 10mL (5U/120mL) of the IL-4 supplemented medium was added to the microglial cells. Microglial cells were incubated for 3 days in a 37°C incubator at 5% CO_2. After 3 days, the cells were centrifuged for 5 minutes at 13,000 rpm and the media was strained using a 100 μm cell sieve. The previous medium in the astrocyte cell flasks was removed and discarded. 10mL of the microglial supernatant was added to each flask. Cells were then incubated for 3 days in a 37°C incubator at 5% CO_2. After 3 days, the differentiated astrocytes were transferred into new flasks. The cells were maintained in a medium of DMEM/F12, 10% FBS, and 1% Pen/Strep and normal cell culture protocol was followed. Cells were passaged 3-4 times before experimentation. Differentiated astrocytes were seeded onto the hydrogel scaffold at a concentration of 2.50 x 10^5 cells per scaffold. Ischemic conditions were used to induce A2 reactive astrocytic properties.

Integrated Implant

A 12.5 mm diameter x 1 mm thick porous circular disk was designed using previous parameters on Fusion360. It was then printed with polyethylene terephthalate glycol (PETG). For the hydrogel, 10% (w/v) gelatin dissolved in PBS, 2% (w/v) chitosan dissolved in 2% acetic acid, 3% (w/v) silk fibroin in 2% acetic acid was combined in a 3:1:1 ratio. Particles of Chondroitinase ABC (4U) and Nerve Growth Factor (20ng/mL) were

injected into the gel. The hydrogel was chemically crosslinked by adding 1% genipin for 1 hour at room temperature. The implant was rinsed with 1X PBS. Cells were seeded onto the implant at a concentration of 2.50 x 10^5 cells per implant. The implants were integrated for 24 hours to allow for cells to adhere.

SEM Pore Analysis

Gold sputter coating was applied onto the sample for 1 minute and 30 seconds. The coated sample was mounted onto the stub and loaded into the microscope. The magnification was set to 27x, 300x, and 500x and randomized images were taken. Pore size and porosity were analyzed using ImageJ software.

Rheological Frequency Sweep

Calibrate machine. 4fl oz. of the sample was loaded into the sample chamber. The geometry was adjusted so that the sample was centered within the measured area. Run experiment measuring shear rate and stress sweeps.

Swelling and Degradation Assay: The sample was weighed then soaked in 200µL dH_2O for 24 hours. The sample was taken out and weighed. Repeat in a 120-day period. The swelling ratio was calculated using this equation: $SR = m - m_0 / m_0 \times 100\%$.

Biocompatibility Analysis: Using an MTT Assay Kit (Invitrogen), cells were seeded in a 96-well plate at a density of 104–105 cells/well in 100 µL of cell culture medium with compounds tested at 37°C. The plate was cultured in a CO_2 incubator for 24–48 hours. 1 mL of PBS was added to one vial of Component A to make a 12 mM MTT stock solution; vortex or sonicate until dissolved. 10 mL of 0.01 M HCL was added to one tube of SDS (Component B). Mix by inversion or sonication until the SDS dissolves. Once prepared, the solution should be used promptly. The cells were washed by removing the medium and replacing it with 100 µL of fresh medium. 10 µL of the MTT stock solution was added to each well. Plate was incubated for 4 hours at 37°C in a CO_2 incubator. 100 µL of the SDS-HCl solution was added to each well. Plate was incubated for 4 hours at 37°C in a CO_2 incubator. Each sample was mixed by pipetting up and down. Absorbance was read at 570 nm using a microplate reader.

Neuroinflammation Quantification: Using a Mouse IL-1β ELISA Kit (Invitrogen), determine the number of microwell strips required. Microwell strips were washed twice with Wash Buffer. Standard dilution on the microwell plate: 100 µL Sample Diluent, in duplicate, was added to all standard wells. 100 µL prepared standard was added into the first wells and created standard dilutions by transferring 100 µL from well to well. 100 µL was discarded from the last wells. 100 µL Sample Diluent was added, in duplicate, to the blank wells. 50 µL Sample Diluent was added to sample wells. 50 µL of sample was added in duplicate, to designated sample wells. Biotin-Conjugate was prepared. 50 µL Biotin-Conjugate was added to all wells. microwell strips were covered and incubated for 2 hours at room temperature (18° to 25°C). Streptavidin-HRP was prepared. Microwell strips were emptied and washed 4 times with Wash Buffer. 100 µL of diluted Streptavidin-HRP was added to all wells. Microwell strips were covered and incubated 1 hour at room temperature (18º to 25ºC). Microwell strips were emptied and washed 4 times with Wash Buffer. 100 µL of TMB Substrate Solution was added to all wells. Microwell strips were incubated for about 10 minutes at room temperature (18°to 25°C). 100 µL Stop Solution was added to all wells. Absorbance was read at 450 nm using a microplate reader.

Astrocyte Growth and Regeneration Assay: Poly-L-Lysine and nitrocellulose coated 1.6mm glass coverslips were spotted with 2µL aggrecan (0.7 mg/ml) and laminin (5µg/ml) in HBSS-CMF (4 spots per coverslip). After the spots were allowed to dry, the coverslips were incubated with laminin (5µg/mL) in HBSS-CMF at 37ºC for

3 hours. Hypoxic A2 reactive astrocytes were plated at a density of 1,000 cells/cm² in cell medium for 5 days at 37ºC. At 5 days, cultures were fixed in 4% paraformaldehyde in PBS for 30 min. After several rinses in PBS, the coverslips were incubated in blocking solution (5% normal goat serum) for 1h at room temperature and then incubated overnight at 4ºC in primary antibody (Anti-GFAP antibody). Coverslips were rinsed several times in PBS and then incubated in the secondary antibody (goat anti-mouse) overnight at 4ºC. Coverslips were rinsed with PBS again, and mounted on glass slides in the mounting medium. Specimens were examined using a fluorescence microscope. Photos were taken and analyzed using ImageJ software.

Results

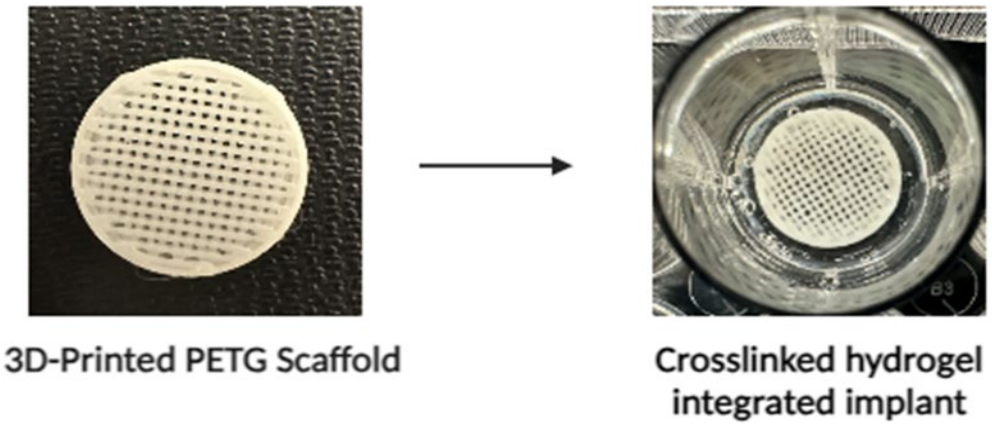

Figure 1. Results of the implant making. The synthetic PETG scaffold is on the left while the chemically cross-linked hydrogel scaffold is on the right.

SEM Pore Analysis

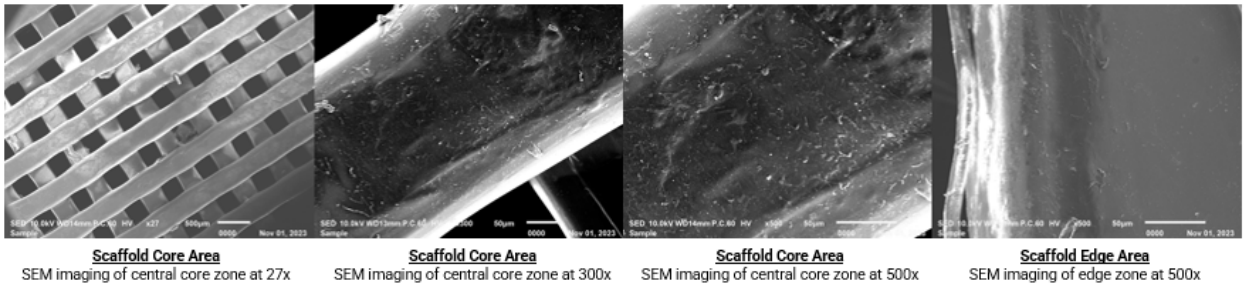

Figure 2. SEM photos at magnification of 27x, 300x, and 500x.

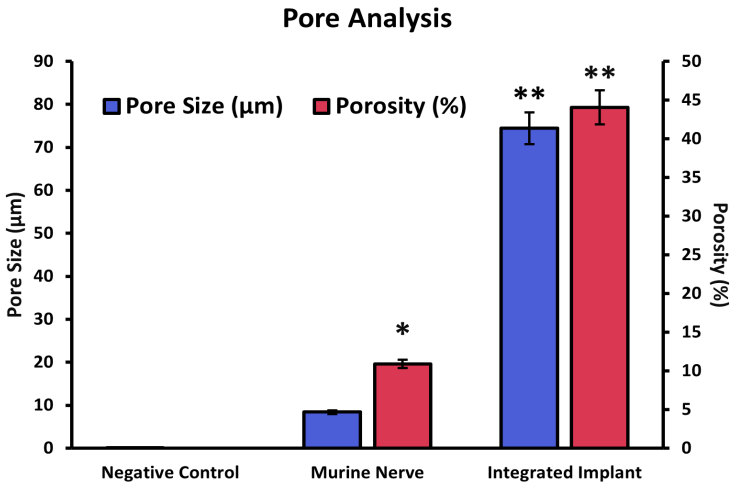

Figure 3. Analysis of pore size and porosity using scanning electron microscopy (SEM). A single asterisk (*) indicates a p-value < 0.05 and a double asterisk (**) indicates a p-value < 0.01 compared to the negative control through Tukey's HSD test.

Randomized images of center and edge zones were taken using Scanning Electron Microscopy (SEM) at magnifications of 27x, 300x, and 500x (Figure 2). Images were analyzed using ImageJ software measuring pore area, feret's diameter, and porosity percentage. The implants had a simple construction and were found to have an average pore area of 74.5µm and a porosity of about 50% conducive to axon growth and lengthening (Figure 3). The implant's pore area and porosity outperformed the nerve graft in a statistically significant difference (One-Way ANOVA, p<0.0001).

Rheological Frequency Sweep

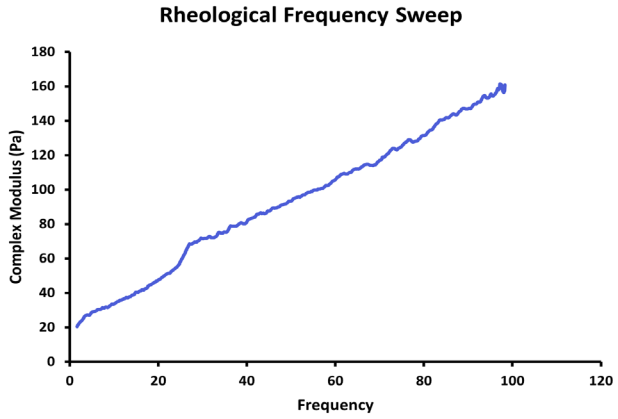

Figure 4. Rheological frequency sweep with complex modulus measured in Pa.

The shear stress, shear strain, and deformation angle were measured through a rheological frequency sweep to capture the complex modulus. The complex modulus is a measurement of how elastic and viscous a substance is when pressure is applied. A linear relationship between the complex modulus was seen as an increasing stress and strain rate was observed (Figure 4). A decreasing deformation angle was observed indicating increasing

solid properties as more pressure is exerted. Overall, the implant had a complex modulus of 162 Pa (One-Way ANOVA, $p<0.05$).

Swelling and Degradation Assay

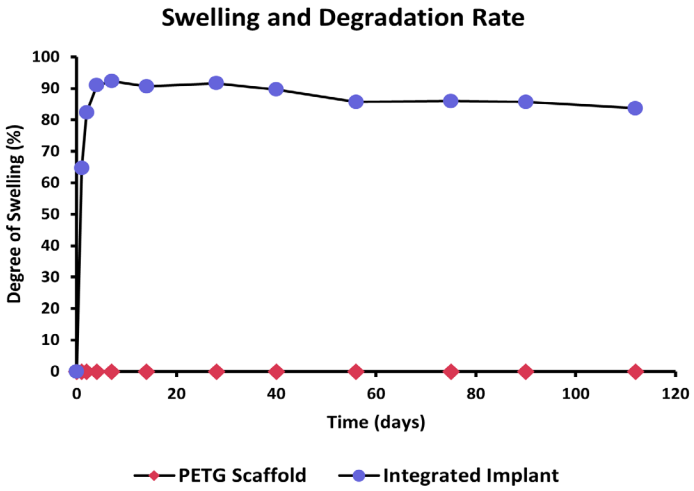

Figure 5. Rate of swelling and degradation using degree of swelling.

After 24 hours, the next measurement would be 48 hours. At 48 hours, the next measurement was 96 hours, and so forth. After 1 month, measurements were taken every two weeks. The integrated implant was able to absorb up to 92% of its dry mass opposed to 0% in the PETG scaffold (Figure 5). The minimal degradation rate within the 120-day period suggests prolonged effectiveness and strong integration when implanted into the human body (One-Way ANOVA, $p<0.01$).

Biocompatibility Analysis

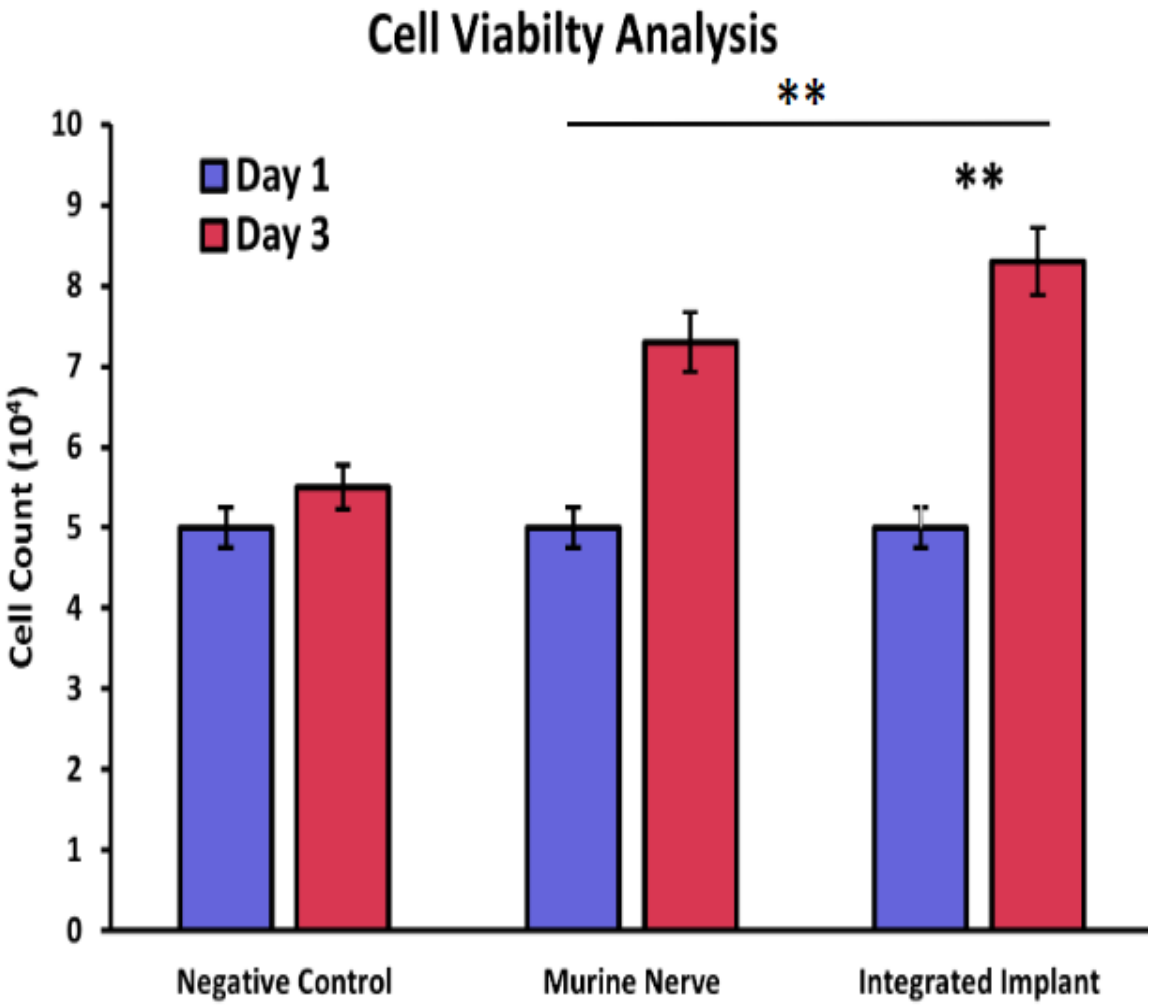

Figure 6. Analysis of cell viability through an MTT assay. A double asterisk (**) indicates a p-value < 0.01 compared to the negative control through Tukey's HSD test.

Cell viability was quantified using an MTT cell viability and proliferation assay. Differentiated A2 reactive astrocyte cells were seeded for 24 hours onto the integrated implant and viability was measured. The integrated implant contained particles of Nerve Growth Factor (NGF), to promote proliferation of cells, and Chondroitinase ABC (ChABC), an enzyme used to remove inhibitory molecules that impede regrowth of nerve fibers and cause tissue scarring. This allowed for 167% proliferation in the integrated implant along with 94% viability which was significantly higher compared to the nerve graft (Figure 6) (One-Way ANOVA, $p<0.01$).

Neuroinflammation Quantification

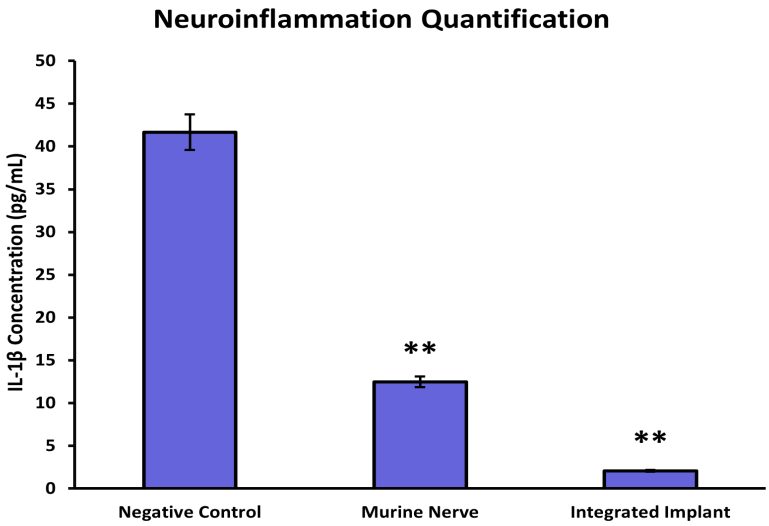

Figure 7. Quantification of neuroinflammation using IL-1β neuroinflammatory markers. A double asterisk (**) indicates a p-value < 0.01 compared to the negative control through Tukey's HSD test.

Neuroinflammation was quantified through an IL-1β ELISA in order to measure the inflammatory response to the implant. IL-1β cytokines are one of the primary modulators of neuroinflammation. A2 reactive astrocytes, anti-inflammatory cells, were seeded for 24 hours before experimenting. The integrated implant had significantly lower levels of inflammation compared to the nerve graft and the negative control at a concentration (pg/mL) of 2.08 against 12.5 in the nerve graft indicating that the implant will minimize neuroinflammation when integrated into the human body (Figure 7) (One-Way ANOVA, $p<0.01$).

Astrocyte Growth and Regeneration Assay

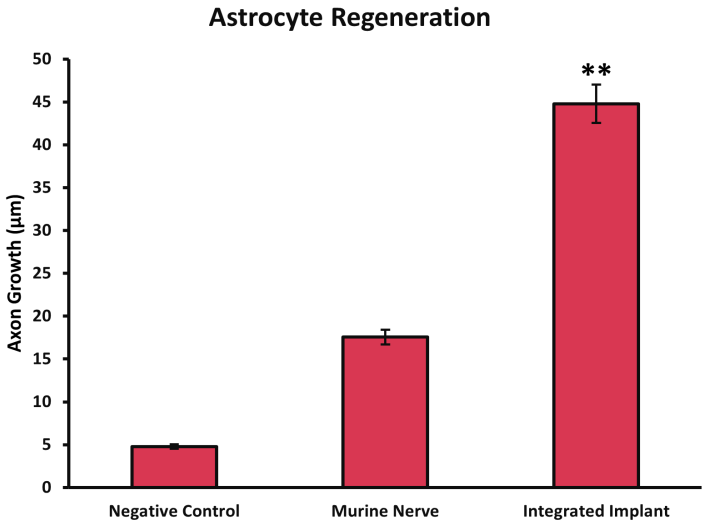

Figure 8. Quantification of astrocyte regeneration across the spot gradient. A double asterisk (**) indicates a

p-value < 0.01 compared to the negative control through Tukey's HSD test.

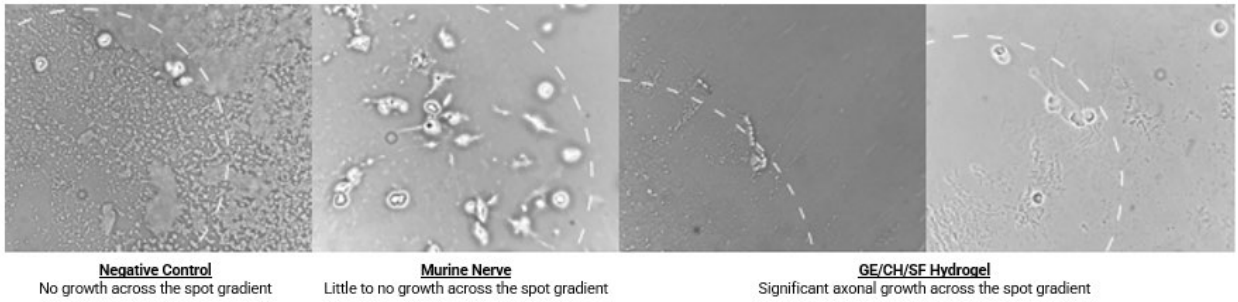

Figure 9. Cell imaging across the spot gradient.

The differentiated astrocytes were seeded onto aggrecan, laminin spotted coverslips and stained using antibodies. An anti-GFAP (glial fibrillary acidic protein) antibody was used to measure axon lengthening and astrocyte regrowth. The axon lengthening across the spot was then measured by taking randomized images and analyzed using ImageJ software. The integrated implant showed the most growth of axon lengths up to 45μm (Figure 8). These were statistically significant to the nerve graft and negative control (One-Way ANOVA, $p<0.01$).

Discussion

SEM Pore Analysis

The hypothesis that the 3D-printed implant would have a pore area of 75-100μm and at least 50% porous was supported. When running statistical analyses, it was found that the implant had significantly higher porosity and pore sizes compared to that of the nerve graft and negative control. This would indicate that the implant can perform significantly better in providing the surface area for the nerves to grow and elongate supporting the engineering goals of a porous implant.

Rheological Frequency Sweep

The hypothesis that the hydrogel implant would have the correct physiological stiffness and elasticity was supported. The shear stress and strain rate increased as frequencies increased indicating a direct relationship between the two. In addition, deformation angle decreased as frequency increased indicating increased stiffness as pressure increased. This is indicative that the implant has fine physical characteristics with capabilities to perform like tissues.

Swelling and Degradation Assay

The hypothesis that the integrated implant would absorb and obtain liquid and degrade at a slow rate was supported. The integrated implant was able to absorb up to 92% of its weight while the PETG scaffold did not absorb any liquid. The integrated implant absorbed its peak of 92% weight at day 28 and then retained liquid until the end of the 120-day period. This displays potential continued effectiveness for years to come. This would support the engineering goal of biodegradable as it will integrate well into the tissue without easily degrading.

Biocompatibility Analysis

The hypothesis that the integrated implant would support cell viability the most and would not induce cytotoxicity was supported. A standard curve was used to quantify cell growth. All groups were found to be non-cytotoxic, but the implant had the largest cell viability at >94%. This performance was significantly better than the nerve graft indicating the implant can improve cell growth much better than the positive control and is biocompatible.

Neuroinflammation Quantification

The hypothesis that the integrated implant would have the lowest amount of neuroinflammation was supported. A standard curve was used to quantify IL-1β cytokines, primary modulators of neuroinflammation. The cells seeded on the implant had significantly lower levels of neuroinflammation at 2.08 pg/mL while the nerve graft and negative control of 12.5 and 41.67 respectively. The quantification of the cytokine shows how there is minimal neuroinflammation as a result of the implant that is usually associated with nerve grafts or implants.

Astrocyte Growth and Regeneration Assay

The hypothesis that the integrated implant would be most conducive for axon lengthening and astrocyte regrowth was supported. ImageJ analysis of the spot gradient measured axon growth across the spot. The implant supported axon growth of 45μm while the nerve graft and negative control had minimal to no growth. This would indicate that the implant has much higher potential for axon regeneration that can not be seen in nerve grafts or any other solution in the field.

Limitations

Limitations of this investigation include budget, model organism constraints, and contamination. More advanced 3D bio ink printers were not able to be utilized due to high costs and advanced maintenance. Biomaterial characterization could be furthered through more in-depth, advanced machinery such as compression testing and transmission electron microscopy. Biological characterization could be enhanced through better testing like confocal microscopy. In addition, human nerve grafts and human cells were not studied due to lab and institution restrictions. Thus, mouse cell lines and mouse nerve grafts were used as an alternative. Neural stem cells were not researched due to high costs and could be utilized to further A2 reactive astrocytic effects. Contamination could have also affected cell viability and growth of astrocytes.

Applications

This investigation contains numerous applications for neural engineering and biomaterial fields. The nervous system is crucial to proper functioning of the entire body. Injury to the nervous system is extremely commonplace with TBIs impacting 55 million worldwide, SCIs affecting 550,000 individuals annually, and PNIs affecting 1 million globally. Injury to the nervous system can often result in cognitive and systemic dysfunction. However, current treatment for central and peripheral nervous system repair exhibits poor efficacy with long-lasting effects, high costs, and limited regeneration leaving societal and economic burdens. This underscores the urgent need for novel interventions.

This novel implant offers a simple, cost-effective fit for patients experiencing any neurological condition or damage. The implant consists of a physiological composition fit for nerve growth and regeneration that

mimics tissue. In addition, the implant reduces the cytotoxicity and inflammation usually associated with nerve autografts and allografts with the addition of NGF and ChABC. The implant is extremely cost-effective, being 300 times less than the industry's current gold standard, nerve autografts. Overall, this novel implant has incredible implications for nerve repair and neural regeneration that can advance the field and improve the quality of life for millions worldwide.

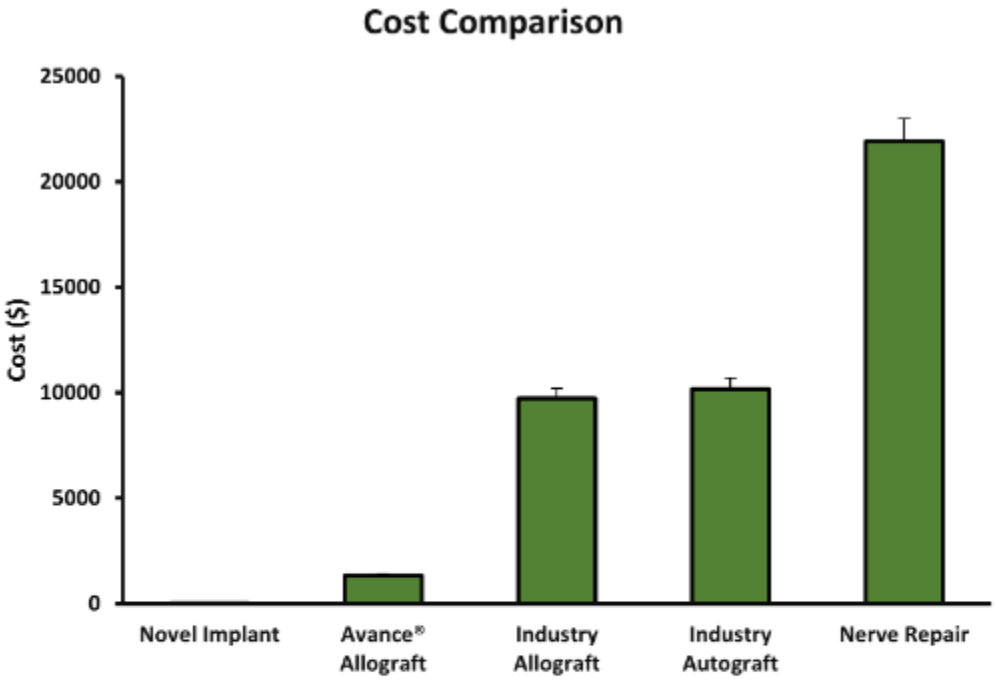

Comparison to Industry Standards	
Gold Standard	**Novel Implant**
Risk of Infection	Non-Cytotoxic
Scarring	Enzymatic Mitigation of Scar Tissue
Inflammatory	Anti-Inflammatory
Healing Complications	Minimally Invasive
Cost: $10,178	Cost: $28.30

Figure 10. Comparison of cost and performance to common industry standards.

Future Research

Future research includes clinical personalization, different biomaterials, and application of regenerative factors. Personalization of implants could be achieved through clinical trials and surveys. Modeling novel implants towards nerves can increase personalization and allow for better integration into the human body. In addition, different biomaterials could be used to enhance biocompatibility, stability, and regenerative properties. The use

of human tissue along with human cell lines could further accuracy and aid integration into the human body, as well as decrease risk of infection from the implant. Application of anti-inflammatory, regenerative cells like the A2 reactive astrocytes in combination with neural stem cells could increase regenerative properties and optimize regeneration of the PNS and CNS.

Acknowledgments

I would like to thank American Heritage Broward for allowing me to work in their lab and Dr. Juliana Caulkins and Dr. Anita Shaw for providing me mentorship throughout the investigation. I would like to thank Dr. Tally Largent-Milnes and Natalie Ricciardi for providing me with the appropriate cell lines. I would like to thank Dr. Courtney Dumont for donating a nerve graft derived from mice. I would also like to thank Jenny Ko and Dr. Dwayne McDaniel for allowing me to utilize their machinery.

References

1. Ansaripour, A., Thompson, A., Styron, J. F., & Javanbakht, M. (2023). Cost–effectiveness analysis of Avance® allograft for the treatment of peripheral nerve injuries in the USA. *Journal of Comparative Effectiveness Research*. https://doi.org/10.57264/cer-2023-0113
2. Centers for Disease Control and Prevention. (2023, May 4). *Stroke Facts*. Centers for Disease Control and Prevention. https://www.cdc.gov/stroke/facts.htm
3. Gallo, V., & Deneen, B. (2014). Glial Development: The Crossroads of Regeneration and Repair in the CNS. *Neuron*, *83*(2), 283-308. https://doi.org/10.1016%2Fj.neuron.2014.06.010
4. Krishani, M., Shin, W. Y., Suhaimi, H., & Sambudi, N. S. (2023). Development of Scaffolds from Bio-Based Natural Materials for Tissue Regeneration Applications: A Review. *Gels*, *9*(2). https://doi.org/10.3390/gels9020100
5. Li, X., Tao, Y., Bradley, R., & Du, Z. (2018). Fast Generation of Functional Subtype Astrocytes from Human Pluripotent Stem Cells. *Stem Cell Reports*, *11*, 998-1008. https://doi.org/10.1016/j.stemcr.2018.08.019
6. Liddelow, S. A., & Barres, B. A. (2017). Reactive Astrocytes: Production, Function, and Therapeutic Potential. *Immunity*, *46*(6), 957-967. https://doi.org/10.1016/j.immuni.2017.06.006
7. Ma, H., Peng, Y., Zhang, S., Zhang, Y., & Min, P. (2022). Effects and Progress of Photo-Crosslinking Hydrogels in Wound Healing Improvement. *Gels*, *8*, 609-629. https://doi.org/10.3390%2Fgels8100609
8. Ohtake, Y., Smith, G. M., & Lu, S. (2016). Reactive astrocyte scar and axon regeneration: suppressor or facilitator? *Neural Regeneration Research*, *11*(7), 1050-1051. https://doi.org/10.4103%2F1673-5374.187022
9. Quan, L., Uyeda, A., & Muramatsu, R. (2022). Central nervous system regeneration: the roles of glial cells in the potential molecular mechanism underlying remyelination. *Inflammation and Regeneration*, *42*(7). https://doi.org/10.1186/s41232-022-00193-y
10. Smith, C. (2018). Neurotrama. *Handbook of Clinical Neurology*, *145*, 115-132. https://doi.org/10.1016/B978-0-12-802395-2.00008-0
11. Subramanian, A., Krishnan, U.M. & Sethuraman, S. Development of biomaterial scaffold for nerve tissue engineering: Biomaterial mediated neural regeneration. *J Biomed Sci*, 108 (2009). https://doi.org/10.1186/1423-0127-16-108

12. Tian L, Prabhakaran MP, Ramakrishna S. Strategies for regeneration of components of nervous system: scaffolds, cells and biomolecules. *Regen Biomater.* 2015 Mar;2(1):31-45. doi: 10.1093/rb/rbu017. Epub 2015 Jan 13.
13. Wong, Z., Liu, H., Luo, W., Li, Z., & Yang, X. (2020). Regeneration of skeletal system with genipin crosslinked biomaterials. *Technological advances in 3D tissue and organ models*, *11*, 1-24. https://doi.org/10.1177%2F2041731420974861
14. World Health Organization. (2007, February 27). *Neurological disorders affect millions globally: WHO report*. https://www.who.int/news/item/27-02-2007-neurological-disorders-affect-millions-globally-who-report
15. World Health Organization. (2013). *Stroke, Cerebrovascular Accident.* https://www.emro.who.int/health-topics/stroke-cerebrovascular-accident/index.html
16. World Health Organization. (2023, November 19). *Spinal cord injury*. World Health Organization. https://www.who.int/news-room/fact-sheets/detail/spinal-cord-injury